J Infrared Milli Terahz Waves (2012) 33:1039–1051
DOI 10.1007/s10762-012-9921-y

Research on Reconstruction Algorithms in 2.52 THz Off–axis Digital Holography

Qi Li · Sheng-Hui Ding · Yun-Da Li · Kai Xue · Qi Wang

Received: 7 May 2012 / Accepted: 21 June 2012 /
Published online: 6 July 2012

Abstract To eliminate the diffraction effect on Terahertz (THz) imaging and improve imaging system performance, digital holography has been investigated. The size of the common THz digital hologram and the recording distance are in the same order of magnitude, which does not satisfy the Fresnel approximation conditions. Meanwhile, diffraction has a great impact on free–space propagation behavior. So the research of the influence on reconstruction performance with different reconstruction algorithms is necessary. In this paper, the numerical simulations of the recording and reconstruction process of 2.52 THz off–axis digital holography imaging have been done, and the reconstruction performances of Fresnel angular spectrum algorithm, Rayleigh–Sommerfeld convolution algorithm and angular spectrum algorithm have been compared and analyzed as the reconstruction reference wave is different. The real experimental reconstruction results have also been presented.

Keywords Holography · THz imaging · Digital hologram

1 Introduction

Terahertz (THz) imaging based on 2D array detector has the capability of real–time imaging which has great application value in a number of fast imaging domains [1–4]. THz wave suffers from the diffraction effect in space propagation because of its long wavelength. Although focal plane imaging can eliminate diffraction effect to some extent, the involvement of the lens will increase the difficulty of the system design and construction, which will also lead to energy attenuation and some distortions. Moreover, as to the traditional focal plane imaging mode, the system focus is fixed so the focal plane is also settled. When the position of the object and

Q. Li (✉) · S.-H. Ding · Y.-D. Li · K. Xue · Q. Wang
National Key Laboratory of Science and Technology on Tunable Laser, Harbin Institute of Technology,
P. O. BOX 3031, No.2 Yikuang Street, Harbin, Heilongjiang, China 150081
e-mail: hit_liqi@yahoo.cn

Qi. Li
e-mail: hit_liqi@sina.com

detector is changed, diffraction will lead to a serious distortion of the imaging results. These factors would degrade the resolution of traditional focal plane imaging system. THz digital holography makes it possible to choose the focal plane freely. The amplitude and phase information can be obtained concurrently from the hologram, and numerical compensator is imported to reduce distortion in the imaging process, which would effectively break the limit of diffraction on imaging resolution availably and have the high–resolution imaging potential [5].

Numerous experimental researches on scanning and array imaging THz digital holography have been undertaken all around the world so far [6–12]. The main parameters in THz digital holographic recording and reconstruction process are clearly different from visible light digital holography. In high–resolution THz digital holographic imaging, the recording distance z_0 is in the same order of magnitude with the dimensions of the hologram, and Fresnel approximation is no longer valid. Diffraction has a greater impact on free–space propagation behavior than visible light. It is necessary to carry out THz digital holography numerical simulations of the effect of different reconstruction algorithms on reconstruction results, which would provide guidance for THz digital holography experiments.

One of the common digital holography reconstruction algorithms is the convolution algorithm (CA) based on Rayleigh–Sommerfeld diffraction integral formula and linearity system theory [13]. Another algorithm is the angular spectrum (AS) algorithm based on angular spectrum diffraction theory [13]. The diffraction plane sampling distance of the convolution algorithm and angular spectrum algorithm is independent of z_0 and wavelength, which only relies on the sampling distance in the object plane. In this paper, the research focuses on the reconstruction impact of the convolution algorithm and angular spectrum algorithm on 2.52 THz digital holography when the reconstruction reference wave is different. The real THz hologram has also been numerically reconstructed.

2 Principle of numerical reconstruction algorithms

2.1 Convolution algorithm

As the direct calculation of the Rayleigh–Sommerfeld diffraction integral formula is complex, Demetrakopoulos *et al.* [14] proposed a convolution algorithm based on the linearity system theory applied to the sub optical holograms.

Rayleigh–Sommerfeld integral can be regarded as the convolution of the light field distribution $U(x, y, 0)$ and system pulse response function $h(x, y, z)$, that is

$$U(x,y,z) = U(x,y,0)*h(x,y,z) \tag{1}$$

$$h(x,y,z) = \frac{\exp\left\{ikz\left[1+(x/z)^2+(y/z)^2\right]^{1/2}\right\}}{i\lambda z\left[1+(x/z)^2+(y/z)^2\right]} \tag{2}$$

Based on the convolution theory, the integral can be expressed as:

$$U(x,y,z) = F^{-1}\left\{F\{U(x,y,0)\}H_R\left(f_x,f_y,z\right)\right\} \tag{3}$$

where $F\{\}$ and $F^{-1}\{\}$ represent Fourier transform and inverse transform, respectively. $H_R(f_x, f_y,z)$ is the Fourier transform of $h(x,y,z)$ in x–y plane, which is the systematic Rayleigh–Sommerfeld diffraction transfer function.

In practice, to simplify calculation, the Fresnel approximation is applied to the integral above. The Fresnel approximation condition is as follows:

$$z^3 >> \frac{\pi}{4\lambda}\left(x^2+y^2\right)^2_{\max} \tag{4}$$

The algorithms using $h_F(x,y,z)$ and $H_F(f_x,f_y,z)$ are called the Fresnel convolution algorithm and Fresnel angular spectrum (FAS) algorithm, respectively. The systematic pulse response function $h_F(x,y,z)$ and the corresponding Fourier transform $H_F(f_x,f_y,z)$ are expressed as follows:

$$h_F(x,y,z) = \frac{\exp(ikz)}{i\lambda z}\exp\left[\frac{ik}{2z}\left(x^2+y^2\right)\right] \tag{5}$$

$$H_F\left(f_x,f_y,z\right) = \exp\left\{ikd\left[1-\frac{\lambda^2}{2}\left(f_x^2+f_y^2\right)\right]\right. \tag{6}$$

where $H_F(f_x,f_y,z)$ is the systematic Fresnel diffraction transfer function.

As the Fourier transform can be approximated by the discrete Fourier transform, the diffraction integral can be approximately evaluated by the use of the discrete Fourier transform. It is necessary to consider that whether the discrete sampling of the transfer function satisfies the Nyquist sampling theory. Suppose that the sampling area is $X \times Y$ in the object plane, the spacing of the sampling point is $\Delta x \times \Delta y$, and the sampling number is $N \times M$ and that is $X \times Y = N\Delta x \times M\Delta y$. The sampling of the systematic pulse response function has to satisfy Nyquist sampling theorem to yield an aliasing–free holographic reconstruction which could be represented as the following function when the convolution algorithm is utilized to calculate the Rayleigh–Sommerfeld diffraction [15]:

$$\frac{|z|}{X} \geq \begin{cases} \sqrt{\frac{1}{(\lambda/\Delta x)^2}-\frac{1}{4}\left[\left(\frac{Y}{X}\right)^2+1\right]}, if \frac{Y}{X}\frac{\Delta y}{\Delta x} \leq 1 \\ \sqrt{\frac{(Y/X)^2(\Delta y/\Delta x)^2}{(\lambda/\Delta x)^2}-\frac{1}{4}\left[\left(\frac{Y}{X}\right)^2+1\right]}, if \frac{Y}{X}\frac{\Delta y}{\Delta x} \geq 1 \end{cases} \tag{7}$$

2.2 Angular spectrum algorithm

The fundamental idea of the angular spectrum algorithm is that the light wave field in object plane is disassembled to the superposition of the plane waves propagating along different directions with different weights. The theory is an accurate description of the diffraction problem. The algorithm applies the Fourier transform to the monochromatic light wave field in the x–y plane firstly, and then the incident light wave is regarded as the superposition of the plane waves propagating along different directions. The superposition weight is represented as follows:

$$A\left(f_x,f_y,0\right) = \int_{-\infty}^{\infty}\int_{-\infty}^{\infty} U(x,y,0)\exp\left[-i2\pi\left(xf_x+yf_y\right)\right]dxdy = F\{U(x,y,0)\} \tag{8}$$

To a monochromatic plane wave whose amplitude is u_0 and space frequency is (f_x,f_y,f_z), the complex amplitude is:

$$u(x,y,z) = u_0 \exp\left[i2\pi\left(xf_x + yf_y + zf_z\right)\right] = u(x,y,0)\exp\left(i\frac{2\pi}{\lambda}z\sqrt{1-\lambda^2f_x^2-\lambda^2f_y^2}\right) \quad (9)$$

As a plane wave whose amplitude is u_0 and space frequency is (f_x,f_y,f_z) in z=0 plane propagates a distance of z, the complex amplitude equals to the product of the complex amplitude in z=0 and the corresponding phase factor:

$$\begin{aligned} A(f_x,f_y,z) = {} & \exp\left(i\tfrac{2\pi}{\lambda}z\sqrt{1-\lambda^2f_x^2-\lambda^2f_y^2}\right)\times \\ & \int_{-\infty}^{\infty}\int_{-\infty}^{\infty}U(x,y,0)\exp\left[-i2\pi\left(xf_x+yf_y\right)\right]dxdy \end{aligned} \quad (10)$$

$$\begin{aligned} U(x,y,z) &= F^{-1}\left\{A\left(f_x,f_y,z\right)\right\} \\ &= F^{-1}\left\{A\left(f_x,f_y,0\right)\exp\left(i\tfrac{2\pi}{\lambda}z\sqrt{1-\lambda^2f_x^2-\lambda^2f_y^2}\right)\right\} \\ &= F^{-1}\left\{F\{U(x,y,0)\}\exp\left(i\tfrac{2\pi}{\lambda}z\sqrt{1-\lambda^2f_x^2-\lambda^2f_y^2}\right)\right\} \end{aligned} \quad (11)$$

It can be inferred that the propagation process of light wave from the diffraction plane to the observation plane in free space is equivalent to passing through an ideal low–pass filter whose cut–off frequency is f=1/λ in frequency domain. The transfer function is:

$$H_A\left(f_x,f_y,z\right) = \exp\left(i\frac{2\pi}{\lambda}z\sqrt{1-\lambda^2f_x^2-\lambda^2f_y^2}\right) \quad (12)$$

The sampling condition must be satisfied when using the angular spectrum algorithm [15]:

$$\frac{|z|}{X} \le \begin{cases} \frac{Y}{X}\frac{\Delta y}{\Delta x}\sqrt{\frac{1}{(\lambda/\Delta x)^2}-\frac{1}{4}\left[\left(\frac{Y}{X}\right)^2+1\right]} & , \quad if \quad \frac{Y}{X}\frac{\Delta y}{\Delta x}\le 1 \\ \sqrt{\frac{1}{(\lambda/\Delta x)^2}-\frac{1}{4}\left[\left(\frac{Y}{X}\right)^2+1\right]} & , \quad if \quad \frac{Y}{X}\frac{\Delta y}{\Delta x}\ge 1 \end{cases} \quad (13)$$

3 Simulation methods

The off–axis digital holography simulated schematic diagram is shown in Fig. 1. In the path x_0–y_0 plane is the object plane and x–y plane is the recording path. The reference wave propagates along z' axis direction, and the angle between z' axis and z axis is θ whose projected angles are θ_x and θ_y in y–z plane and x–z plane, respectively. We suppose that the reference wave and object wave are all fundamental mode Gaussian beams, the position of the beam waist of the object wave is Δz behind the recording plane, and the position of the reference wave beam waist is the point of intersection of z' axis and z axis (the center point of recording plane o). Then the optical path difference of the object wave and reference wave in o is Δz. (k_x,k_y,k_z) is used to represent the plane wave vector propagating along z' axis, and

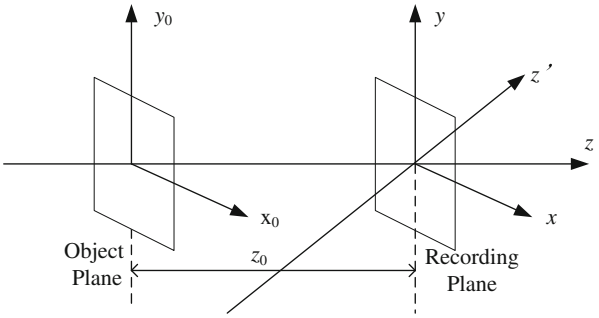

Fig. 1 Off–axis digital holography simulated schematic diagram.

the relations are as follows:

$$\begin{aligned} k_x &= k\sin\theta_x = (2\pi\sin\theta_x)/\lambda \\ k_y &= k\sin\theta_y = (2\pi\sin\theta_y)/\lambda \\ k_z &= \sqrt{k^2 - k_x^2 - k_y^2} = k\cos\theta \end{aligned} \tag{14}$$

To obtain the complex distribution of the reference wave in the recording plane, the propagation parameter (r,z) of the Gaussian beam is calculated with the coordinates transformation function (15) firstly. Then the propagation parameter is substituted in the fundamental mode Gaussian beam function (16) to obtain the corresponding complex amplitude distribution of the reference wave in the recording plane.

The simulation method to achieve holograms is as follows:

(1) The complex amplitude distribution $i(x_0,y_0)$ in the object plane can be obtained based on the fundamental mode Gaussian beam function. By multiplying it by the transmissivity parameter $t(x_0,y_0)$ of the simulation object, the complex amplitude distribution of the light field in the object plane is obtained. Then the diffraction distribution $O(x,y)$ in the recording plane is calculated with the diffraction integral function (1).
(2) By use of the coordinates transformation function (15) the corresponding coordinate (r',z') in the reference wave coordinate system of (x,y) in the recording plane is obtained. The complex amplitude distribution $R(x,y)$ of the reference wave in the recording plane is achieved by substituting (r',z') in the fundamental mode Gaussian beam function (16).
(3) The field intensity distribution in the recording plane is calculated based on $I(x,y) = |O(x, y) + R(x,y)|^2$, and the hologram is obtained by sampling the filed distribution $I(x,y)$.

The coordinates transformation function and fundamental mode Gaussian beam function are shown as follows:

$$(x,y) \rightarrow \begin{cases} z' = \frac{k_x x + k_y y}{2\pi/\lambda}, \\ r' = \left(x^2 + y^2 - z'^2\right)^{1/2} \end{cases} \tag{15}$$

$$E(r,z) = \frac{E_0}{w(z)} \exp\left[-r^2/w^2(z)\right] \exp[i\varphi_{00}(r,z)] \tag{16}$$

Where $w(z)$ represents the beam radius when the Gaussian beam propagates a distance of z, $w(z) = \omega_0[1 + (z/f)^2]^{1/2}$. f is the confocal parameter of the Gaussian beam, and φ_{00} is the phase factor:

$$\varphi_{00}(r,z) = k\left(z + \frac{r^2}{z + f^2/z}\right) - \arctan\frac{z}{f} \tag{17}$$

The chosen parameters in the simulation are: the light frequency is 2.52 THz (118.8 μm), the angle between z' axis and z axis is θ=24.8°,θ_x=θ_y=17.3°. The reference wave and object wave are all fundamental mode Gaussian beams whose beam waist is 6.5 mm, the position of the beam waist of the object wave is Δz=10 cm behind the recording plane, and the amplitude ratio of the reference wave and object wave is 1:1.5. The chosen sampling number $M \times N$ is 1024×1024 when computing the diffraction field of the object wave and reference wave, and the sampling spacing $\Delta x \times \Delta y$ is 0.02 mm×0.02 mm, which means that the sampling area is $X \times Y$=20.48 mm×20.48 mm. The interference pattern in the recording plane is shown in Fig. 2(a) when there is no object in the object plane. We supposed that the size of the detector in the recording plane is 12.4 mm×12.4 mm, the pixel number is 124×124, the size of the photosurface cell is 0.08 mm×0.08 mm, and the interval between the pixel center is $\Delta x = \Delta y$=0.1 mm. It is supposed that every photosurface cell responds uniformly to the incident light and the light outside the cell doesn't interfere with the photosurface. The detection process corresponds to the downsampling of the interference field distribution in the recording plane after a mean filter with a window of 4×4 pixels. The simulation result is shown in Fig. 2(b).

4 Influence of different reconstruction reference wave

The simulation object is shown in Fig. 3(a), and intervals of the stripe arrays are 0.6, 0.4, 0.3, 0.2 and 0.1 mm from left to right. The object size is 12.8 mm×12.8 mm. The transmissivity of the white area is 1 and the transmissivity of black area and the exterior area is 0. The object is placed 3 cm in front of the detector, and the transmitting light field is shown in Fig. 3(b). According to function (7), the following sampling condition must be satisfied when the convolution algorithm is used to calculate the Rayleigh–Sommerfeld diffraction function:

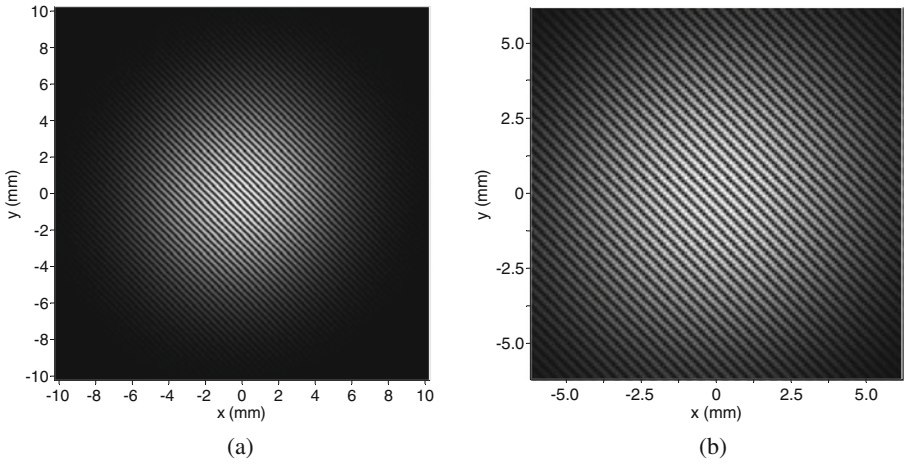

Fig. 2 Simulation results of the interference field distribution and the recording result: (**a**) interference field distribution in the recording plane; (**b**) recording result by the detector.

$$\Delta x \le \lambda \left[1/2 + (z/X)^2\right]^{1/2} \tag{18}$$

As the sampling interval fulfils $\Delta x \le (\lambda/2)$ the convolution algorithm is the same with diffraction calculation of random distance. Then the convolution algorithm is utilized all the time. The hologram based on the method mentioned in Section 3 is shown in Fig. 3(c).

The Fourier transform is applied to the hologram and the frequency spectrum is shown in Fig. 3(d). To enhance the gray level details, The logarithm transform is utilized to the Fourier frequency spectrum ($f' = \ln(1+f)$). The center coordinates of the zero–order and ±1–order diffraction frequency spectrum are (63, 63), (32, 94) and (94, 32), respectively, which represents that the center of ±1–order diffraction frequency spectrum locates in the center of the first quadrant and third quadrant, respectively. In case of meeting the Nyquist sampling theory, the highest cut–off frequency of the object wave that can be recorded is $1/(4\Delta x)$, and k_x, k_y and k_z are as follows:

$$\begin{aligned} k_x &= \frac{2\pi(63-32)}{124\times 0.1}(\mathrm{mm}^{-1}) = 15.71\mathrm{mm}^{-1} \\ k_y &= \frac{2\pi(63-102)}{124\times 0.1}(\mathrm{mm}^{-1}) = -15.71\mathrm{mm}^{-1} \\ k_z &= \sqrt{\left(\frac{2\pi}{\lambda}\right)^2 - k_x^2 - k_y^2}(\mathrm{mm}) = 47.98\mathrm{mm}^{-1} \end{aligned}$$

In practice, the complex amplitude distribution of the reference light is hard to obtain, and then the reconstruction reference light is replaced by the plane wave or spherical wave approximately. The plane wave propagating along the object wave and plane wave along the conjugate direction are two common approximations. In this paper, the beam waist is relatively large and the divergence angle is small, then the plane wave is utilized as the reference wave approximately.

To choose appropriate diffraction calculation algorithm, the applicable conditions of the Fresnel approximation, the convolution algorithm based on Rayleigh–Sommerfeld diffraction integral and the linearity system theory and the angular spectrum diffraction theory are taken into account. Based on Eqs. (4), (7) and (13), the sampling interval is 0.1 mm and X= 51.2 mm, and then the applicable conditions are: the Fresnel approximation $z_0 >> 224.8$ mm, the convolution algorithm based on Rayleigh–Sommerfeld diffraction integral $z_{0\min}$= 23.4 mm, the angular spectrum algorithm $z_{0\max}$=23.4 mm.

It can be inferred that the chosen simulation parameters make the algorithms locate in the boundary of the applicable scope on THz wave band. It is necessary to compare and analyze the reconstruction performance of these algorithms. The plane wave propagating along the object wave (noted as R_1) and plane wave whose wave vector is $(-k_x,-k_y,k_z)$ (noted as R_2) are

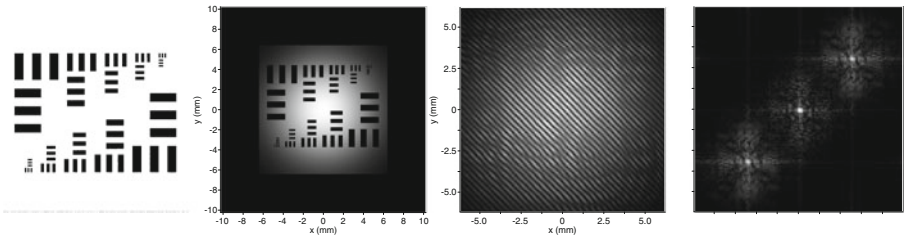

Fig. 3 Simulation object and recorded hologram: (**a**) simulation object; (**b**) transmitting field distribution; (**c**) recorded hologram; (**d**) frequency spectrum of the hologram.

utilized as the reconstruction reference waves. The reconstruction results using the FAS, CA and AS are shown in Figs. 4 and 5. The reconstruction results are all intensity images in this paper.

It can be inferred in Figs.4 and 5 that the zero–order diffraction occupies most of the light energy, which makes the reconstructed object dingy and grey level details mixed in the reconstruction image. By the use of the plane wave R_1 to reconstruct, there is distortion in the reconstruction result with these three algorithms. The results using CA and AS have worse distortions and blurs. The result using FAS has a distortion. However, the left bottom area is fuzzy. When the plane wave R_2 is used, the results using three algorithms are preferable except that there is slight distortion in the 0.2 mm stripe far away from the image center.

The plane wave is used as the object wave and reference wave in the simulation to search the reason of a distortion, and the results are shown in Fig. 6(a)–(d) and (e)–(h). They are the recorded hologram, the FAS, CA and AS results from left to right. The plane wave whose wave vector is $(-k_x,-k_y,k_z)$ obtained from the hologram Fourier frequency spectrum is used as the reconstruction reference wave. The reconstruction result still has a distortion as the object wave is plane wave. Most of the distortion is eliminated except a portion distortion in the left bottom when the reference wave is plane wave. It can be inferred that the main reason caused the distortion is the approximation to use the plane wave as reference wave. Using the plane wave as an approximation of the Gaussian beam will lead to some distortion in the reconstruction image. It is necessary to ensure the recording wave has relatively preferable uniformity to reduce the reconstruction distortion when the plane wave is used as the reference wave.

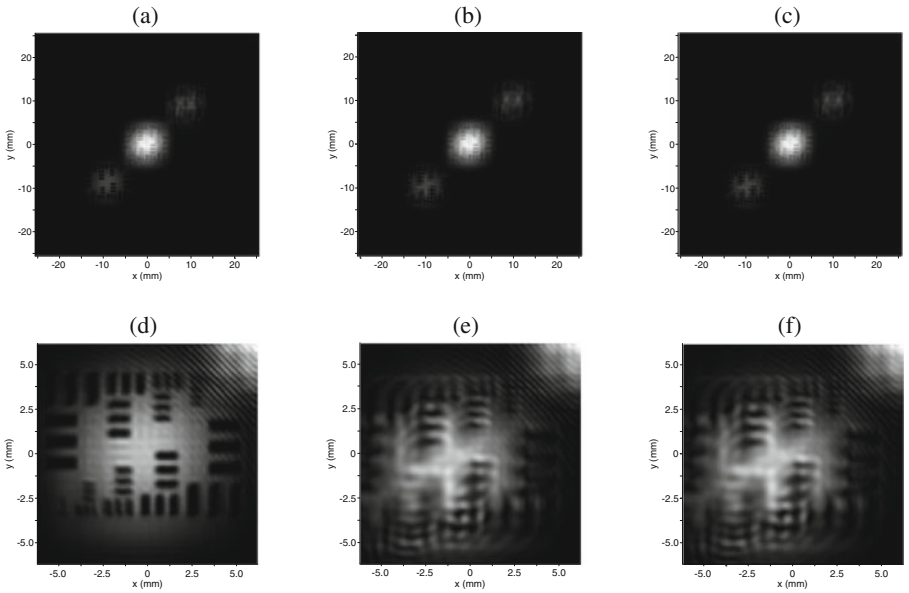

Fig. 4 Reconstruction results using plane wave R_1: (**a**) FAS result; (**b**) CA result; (**c**) AS result; (**d**) cropped from (**a**); (**e**) cropped from (**b**); (**f**) cropped from (**c**).

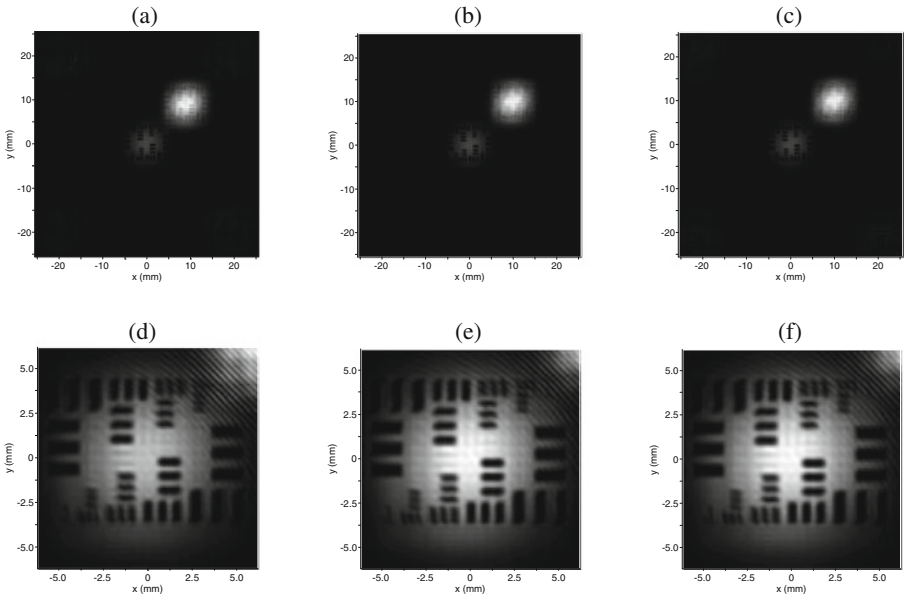

Fig. 5 Reconstruction results using plane wave R_2: (**a**) FAS result; (**b**) CA result; (**c**) AS result; (**d**) cropped from (**a**); (**e**) cropped from (**b**); (**f**) cropped from (**c**).

Furthermore, compared with the results using the other two algorithms, the FAS result suffers badly from the zero–order diffraction. The reason is that the distance between the –1–order diffraction and zero–order diffraction is shorter than those of the other two algorithms. Synthetically consider the reconstruction results using the

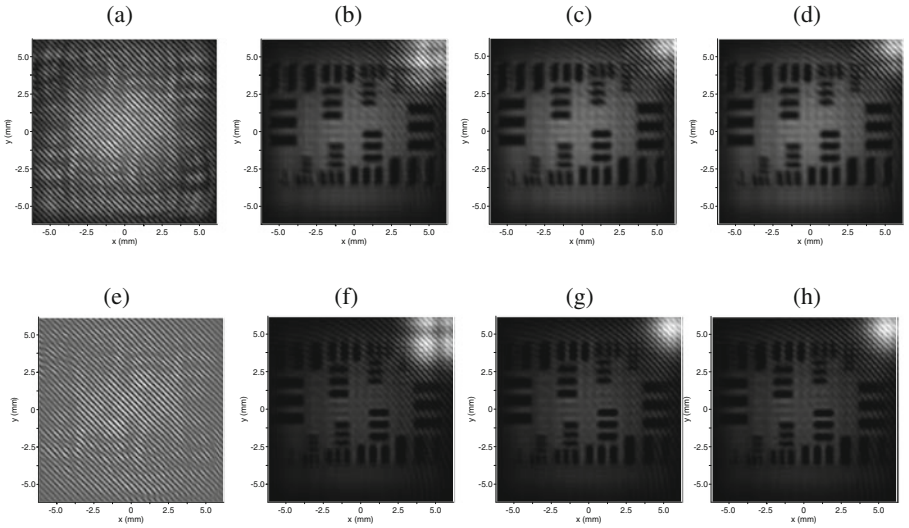

Fig. 6 Holograms and reconstruction results as plane wave and reference wave are plane wave: (**a**) object wave is plane wave; (**b**) FAS result; (**c**) CA result; (**d**) AS result; (**e**) reference wave is plane wave; (**f**) FAS result; (**g**) CA result; (**h**) AS result.

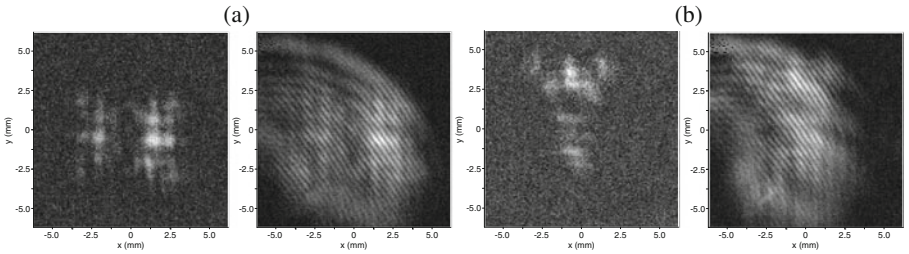

Fig. 7 Object wave and holograms of letters 'H' and 'T': (**a**) object wave and holograms of letter 'H'; (**b**) object wave and holograms of letter 'T'.

plane wave propagating along the object wave as the reconstruction reference wave (Fig. 4), we can conclude that the reason is the use of paraxial approximation in Fresnel approximation calculation. The result can approximate to a paraboloid surround the hologram, and then the distance between the off–axis image and the holography plane is nearly z_0. For the other two algorithms, the result is a plane whose propagating distance is z. When the reconstruction wave propagates along the

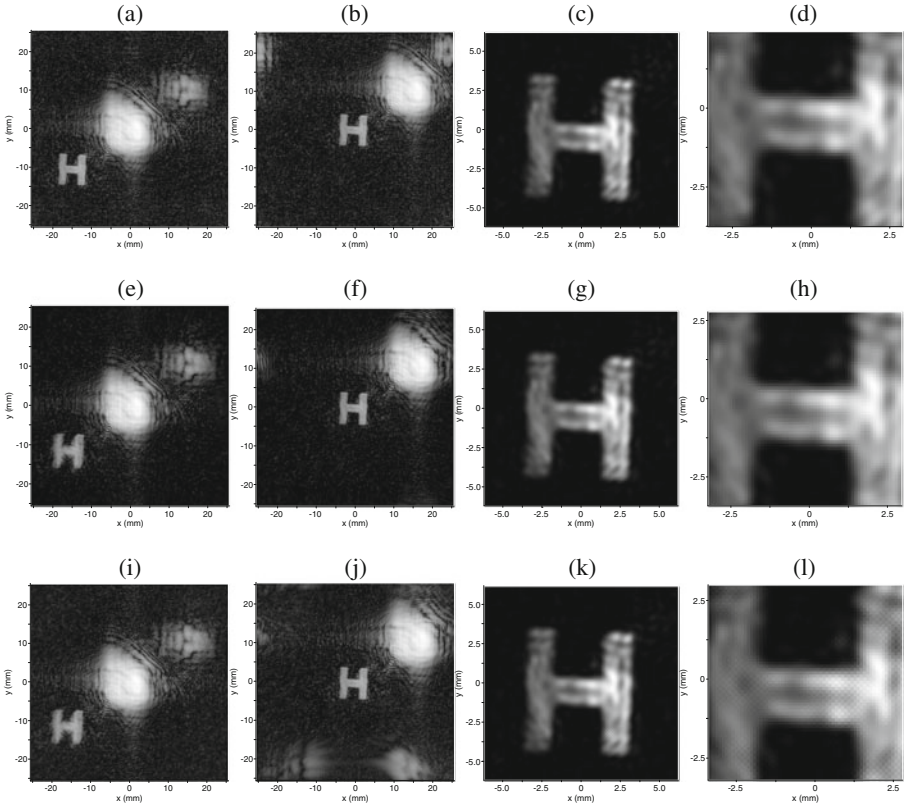

Fig. 8 Hologram and reconstruction result of 'H'. (**a**) FAS, R_1; (**b**) FAS, R_2; (**c**) –1–order diffraction from (**b**); (**d**) cropped from (**c**); (**e**) CA, R_1; (**f**) CA, R_2; (**g**) –1–order diffraction from (**f**); (**h**) cropped from (**g**); (**i**) AS, R_1; (**j**) AS, R_2; (**k**) –1–order diffraction from (**j**); (**l**) cropped from (**k**).

object wave, the main axis direction of –1–order diffraction is the same as the reference wave used in hologram recording, which is (k_x,k_y,k_z). Then the linear distance between –1–order diffraction image and the hologram is larger than z_0, and the calculation result is not perpendicular to the main axis direction. So the reconstruction result is the diffraction projection of the real image in the reconstruction plane. Based on this, it is obvious that the distance between –1–order diffraction and zero–order diffraction using the Fresnel approximation is shorter than the real distance as the reconstruction reference wave propagating along the conjugate direction. In practice, it is necessary to take the incident direction of reconstruction reference wave into account to reduce the distortion.

5 Reconstruction results of the real imaging

The experimental system [1, 8] is utilized to image a hollowed aluminium plate which has letters 'H' and 'T' in it. The THz source is a SIFIR-50 laser (Coherent, Inc). The pyroelectric array camera is a Pyrocam III (Ophir-Spiricon, Inc). To expand the laser, four goldcoated off–axis parabolic mirrors are utilized. Highresistivity silicon wafers are employed as beam splitters. The recorded object wave and holograms are shown in Fig. 7. In our experiments, the recording holograms are all 10–frame averaging results. The object is placed 4.7 cm in front of the detector photosurface. It can be inferred that after a propagating distance of 4.7 cm, the object wave arriving at the photosurface suffer badly from diffraction, and the object characters is hard to distinguish.

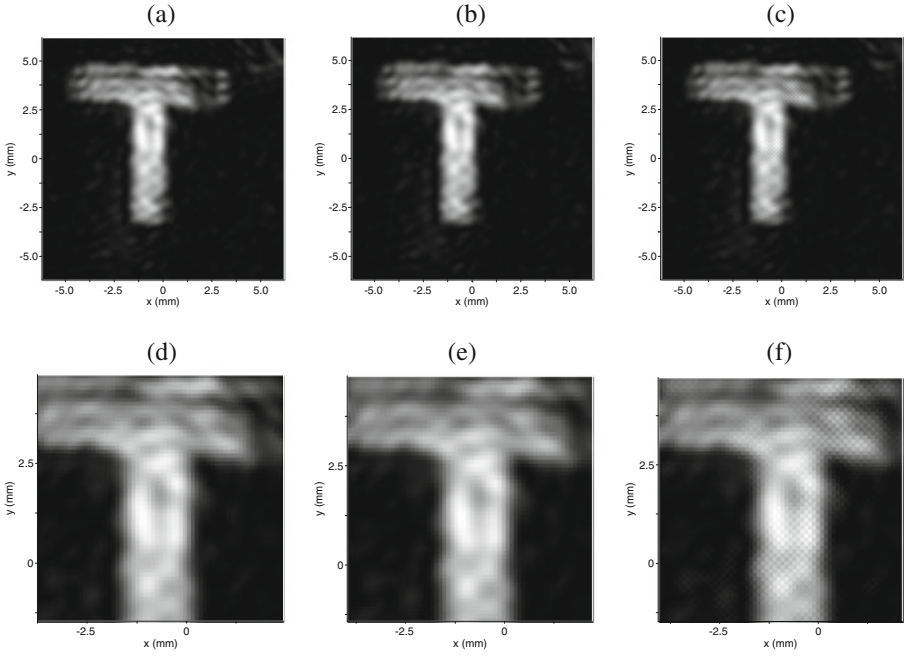

Fig. 9 Hologram and reconstruction result of letters 'T'. (**a**) FAS result; (**b**) CA result; (**c**) AS result; (**d**) cropped from (**a**); (**e**) cropped from (**b**); (**f**) cropped from (**c**).

The FAS, CA and AS combined two reference waves R_1 and R_2 are utilized to reconstruct letter 'H', and the result is shown in Fig. 8. The logarithm transformation is used to enhance image details in (a)–(b), (e)–(f), (i)–(j). As z_0 and the intervals of different order diffraction are all large, the zero–order diffraction can be eliminated by cutting off the calculation result. Similar to the simulation conclusion, the reconstruction results using the CA and AS have serious distortion when the reconstruction reference wave is R_1. It can be inferred by way of the local magnifier of the –1–order diffraction that the result using the AS has severe image degradation. That is because that the reconstruction distance 4.7 cm is far greater than the applicable range. While the result using the other two algorithms has less distortion. When the reference wave is R_2, there is visible rhombus aberration on the surface of the reconstructed 'H' using the AS. The image quality using CA and FAS is similar, however, the uniformity in the reconstructed 'H' using FAS is slightly bad. The reasons of the unconspicuous difference are that the object is much smaller than the simulation model, the recording distance is longer and the details are also less.

The letter 'T' is used to image and reconstruct. Three algorithms are utilized and R_2 is used as the reconstruction reference wave, and the reconstruction results are shown in Fig. 9. The result is similar to that of the 'H'. It can be inferred that there is also no obvious difference in the reconstruction results using the FAS and CA, however, the reconstruction result using the AS has revere rhombus aberration on the surface. It is necessary to take the applicable range of the algorithms into account to obtain optimal reconstruction performance and operation efficiency.

6 Conclusion

The numerical simulation and experiments have been carried out to investigate the recording and reconstruction process of THz digital holography in this paper. It can be inferred from the reconstruction results that when the recording distance is located in the critical range of these algorithms, the improper choice of reconstruction algorithm will cause severe image degradation. So it is essential to choose optimal reconstruction algorithm based on the real experimental parameters. The approximation to use the plane wave to replace the Gaussian beam will lead to some distortion. The choice of the reconstruction reference wave is significant to the reconstruction process, and the improper incident direction will bring serious distortion. In practice, choosing proper incident direction to reduce aberration is important. As the behavior of THz digital holography is different from that in visible domain, the comparison research on reconstruction performance of different algorithms which has not been done before is of great significance.

Acknowledgements This work was supported by the Specialized Research Fund for the Doctoral Program of Higher Education (SRFDP) of China 20112302110028.

References

1. R. S. Albert, and X. –C. Zhang, "Terahertz science and technology trends," IEEE J. Sel. Top. Quant. Elect. 14(2), 260–269 (2008).
2. P. W. Vincent, M. P. Emma, J. A. Zeitler, and R. Caroline, "Three–dimensional imaging of optically opaque materials using nonionizing terahertz radiation," J. Opt. Soc. Am. A 25(12), 3120–3133 (2008).
3. W. M. Lee Alan, and Qing Hu, "Real–time, continuous–wave terahertz imaging by use of a microbolometer focal–plane array," Optics Letters 30(19), 2563–2565 (2005).

4. Q. Li, Y. D. Li, S. H. Ding, Q. Wang, "Terahertz Computed Tomography Using of a Continuous–Wave Gas Laser," J Infrared Milli Terahz Waves 33, 548–558 (2012).
5. S. H. Ding, Q. Li, Y. D. Li, Q. Wang, "Continuous–Wave Terahertz Digital Holography by Use of a Pyroelectric Array Camera," Optics Letters 36(11), 1993–1995 (2011).
6. R. Mahon, A. Murphy, W. Lanigan, "Terahertz Holographic Image Reconstruction and Analysis," 29th Int. Conf. on Infrared and Millimeter Waves and 12th Int. Conf. on Terahertz Electronics, 749–750 (2004).
7. B. A. Knyazev, G. N. Kulipanov, N. A. Vinokurov, "Novosibirsk Terahertz Free Electron Laser: Instrumentation Development and Experimental Achievements," Measurement Science and Technology 21(5), 054017 (2010).
8. R. J. Mahon, J. A. Murphy, W. Lanigan, "Digital Holography at Millimetre Wavelengths," Optics Communications 260(2), 469–473(2006).
9. I. McAuley, J. A. Murphy, N. Trappe, R. Mahon, D. McCarthy, P. Mclaughlin, "Applications of Holography in the Millimeter–Wave and Terahertz Region," Proc. of SPIE, 7939, 79380 H (2011).
10. M. S. Heimbeck, M. K. Kim., D. A. Gregory, and H. O. Everitt, "Terahertz Digital Holography Using Angular Spectrum and Dual Wavelength Reconstruction Methods," Optics Express 19(10), 9192–9200 (2011).
11. Y. Zhang, W. Zhou, X. Wang, Y. Cui and W. Sun, "Terahertz Digital Holography," Strain 44(5), 380–385 (2008).
12. Q. Li, S. H. Ding, Y. D. Li, Q. Wang, "Experimental Research on Resolution Improvement in CW THz Digital Holography," Appl. Phys. B 107(1), 103–110 (2012).
13. T. M. Kreis, M. Adams, W. P. O. Jüptner, "Methods of digital holography: a comparison," Proc. SPIE 3098, 224–233 (1997).
14. T. H. Demetrakopoulos, R. Mittra, "Digital and Optical Reconstruction of Images from Suboptical Diffraction Patterns," Applied Optics 13(3), 665–670 (1974).
15. F. DovalÁ, C. Trillo, "Dimensionless Formulation of the Convolution and Angular Spectrum Reconstruction Methods in Digital Holography," Proc. of SPIE, 7387, 73870U (2010).